Research Article Vol. 13, No. 2 / February 2025 / Photonics Research 541

PHOTONICS Research

Low-cost prototype for real-time analysis using liquid crystal optical sensors in water quality assessment

M. Simone Soares,[1,2,†] Francisco Gameiro,[1,†] Jan Nedoma,[3] Nuno Santos,[2] Pedro L. Almeida,[4,5] and Carlos Marques[1,6,*]

[1]CICECO - Aveiro Institute of Materials & Physics Department, University of Aveiro, Aveiro, Portugal
[2]I3N & Physics Department, University of Aveiro, Aveiro, Portugal
[3]Department of Telecommunications, VSB - Technical University of Ostrava, Ostrava, Czech Republic
[4]I3N - CENIMAT, School of Sciences and Technology, NOVA University of Lisbon, Lisbon, Portugal
[5]UnIRE, ISEL, Polytechnic University of Lisbon, Lisbon, Portugal
[6]Department of Physics, VSB - Technical University of Ostrava, Ostrava, Czech Republic
[†]These authors contributed equally to this work.
*Corresponding author: carlos.marques@ua.pt

Received 3 October 2024; revised 4 December 2024; accepted 4 December 2024; posted 6 December 2024 (Doc. ID 543957); published 31 January 2025

In the food production sector, quickly identifying potential hazards is crucial due to the resilience of many pathogens, which could lead to wasted production results and, more severely, epidemic outbreaks. *E. coli* monitoring is essential; however, traditional quality control methods in fish farming are often slow and intrusive, thus promoting an increase in fish stress and mortality rates. This paper presents an alternative method by utilizing a prototype inspired by polarized optical microscopy (POM), constructed with a Raspberry Pi microprocessor to assess pixel patterns and calculate analyte levels. The sensors are based on the immune complexation reactions between *E. coli* specific antibodies and the disruption of liquid crystal (LC) alignment, which are measured with the POM technique. The prototype yielded a sensitivity of 1.01% ± 0.17%/$\log_{10}$ (CFU/mL) for *E. coli*. In this paper, tests using sunlight as the prototype's light source were also performed, and a user-friendly graphical user interface was designed.

https://doi.org/10.1364/PRJ.543957

1. INTRODUCTION

Foodborne infections present a global health challenge; as such, it is critical to ensure the application of rigorous practices regarding food preservation and consumption [1], in order to reduce the spread of infectious diseases. Annually, according to data from the World Health Organization (WHO) and the European Food Safety Authority (EFSA), an occurrence of 600 million cases of foodborne illnesses is estimated. Even though these types of diseases can be caused by the presence of viruses, parasites, and chemicals in food, the most common pathogens are bacteria such as *Salmonella* and *Escherichia coli* (*E. coli*). They can sometimes resist under extreme conditions during long periods, which could facilitate their spread [2–4].

The interest in the pathogenic *E. coli* comes from bivalve harvesting and production all over the world, as it results in the farming of 17.7 million tons of mollusks and 11.2 million tons of bivalves [5], but also more specifically on the Portuguese coast [6]. Since the estuaries expand from the north to the south of the coast, their production has a large socioeconomic impact on the country [7,8]. The aquaculture industry, however, can be severely affected by the presence of these bacteria originating from fecal contamination due to urban activities, industrial waste, etc. [9]. Pathogen contamination poses a serious threat, as these saltwater bivalves, such as oysters and shellfish, are most of the time consumed raw, alive, or undercooked [10]. In the European Union, the legal limits for the safeness of consumption are established by the following rigorous classes according to the presence of *E. coli* concentration [expressed as most probable number (MPN)] in 100 g of bivalve meat: Class A if ≤230 *E. coli* MPN/100 g; Class B if >230 and ≤4600 *E. coli* MPN/100 g; and Class C if >4600 and ≤46,000 *E. coli* MPN/100 g; further, the consumption is forbidden for >46,000 *E. coli* MPN/100 g, according to the Portuguese Institute for Sea and Atmosphere (IPMA) [11].

When managing production systems in the aquaculture sector, two essential factors should be considered to promote a healthy, safe, and sustainable cultivation environment and thus mitigate possible environmental impacts, associated with the

spread of pathogenic microorganisms and the conditions of the production environment. This risk management elevates growth potential and reduces the environmental effects on fish and bivalve production. Therefore, the timely detection of microorganisms of a pathogenic fashion should be of the utmost importance, especially when considering bivalve production in estuaries and cages, as many urban activities could lead to an increase in water pollution [12].

Liquid crystals (LCs) are considered the intermediate state of matter between crystalline solids and isotropic liquids, as they present fluidity and droplet coalescence, while their molecules self-organize in a crystalline molecular structure with similar properties to anisotropic crystals. They are categorized into phases, which can differ in molecular structure while remaining orientated in the same general direction. Its molecules can be elongated, predominantly in the nematic and smectic phases, or have disk-like structures, typically in columnar and some nematic phases [13,14]. These types of materials are sensitive to external stimuli (temperature, electromagnetic fields, and stress variations), and this property can be harnessed to fabricate sensors capable of detecting those changes. The LC-based biosensors in this paper are composed of two functionalized glass surfaces facing each other, with the LC molecules displayed perpendicularly to each other in between those glass plates, similar to the diagram shown in Fig. 1. The LC used is 4-cyano-4'-pentylbiphenyl (5CB) due to its elongated structure and optical anisotropy and remaining at the nematic phase at room temperature [15,16].

The more widespread method of detecting bacteria is via microbiology protocols where the bacteria are grown in culture mediums and identified based on their specific enzyme activities. These procedures normally take at least 24 h to present their results. Using a liquid crystal sensor, the test results are immediate.

In these types of sensors, the LC is homeotropically aligned inside the glass plates, and the results are observed using a polarized optical microscope (POM), which uses two crossed polarizers to analyze birefringent materials, similar to the representation in Fig. 1. When light passes through the first polarizer and there is no presence of bacteria, the liquid crystal molecules remain perfectly aligned perpendicular to the glass, and the incident light will be extinct on the second polarizer, resulting in a negative detection of the analyte. If the *E. coli* bacteria are bonded to the anti-*E. coli* antibodies, the presence of the molecules will distort the liquid crystal molecules' orientation and thus allow the passage of the incident light between cross polarizers [17]. This fast result allows taking action on controlling the contamination much sooner than the traditional methods.

In recent years, several other available methods for pathogenic bacteria detection have been presented. However, most of the methods pose a major drawback regarding their wide accessibility, due to the costly specialized equipment in order to obtain accurate measurement as in the methods presented by Locke *et al.* [18]. Similarly, in Ref. [19] by Wang *et al.* where spectroscopy-based methods are presented such as "surface-enhanced Raman scattering spectroscopy, surface plasmon resonance, and dark-field microscopic imaging techniques," which, with expensive equipment and time-consuming processes, result in a disadvantage for *in situ* applications.

The main contribution of this research is to expand upon previous studies on LC-based biosensors by developing a prototype that addresses the limitations of traditional POM analysis for these sensors [15]. The POM is a robust and expensive device, as its price could range from $1000 US, for simpler microscopes, to over $12,000 US, for microscopes with digital support [20,21], and this prototype aims to reduce the analysis burden associated with this device. It offers a cost-efficient alternative, capable of in-the-field testing and real-time quantification of *E. coli* present in the previously developed LC-based immunosensors. This design maximizes portability and convenience and eliminates the need for lengthy analysis via POM. This research also contributes to addressing and discussing finer solutions on *E. coli* detection and providing a good solution in terms of selectivity for complex media while further exploring the prototype's concept by providing possible ecological alternatives.

2. MATERIALS AND METHODS

A. LC-Based Biosensor Production

The setup was constructed to analyze specific types of LC-based biosensors developed in a previous study [15], designed to detect pathogenic *E. coli*. These sensors are fabricated from

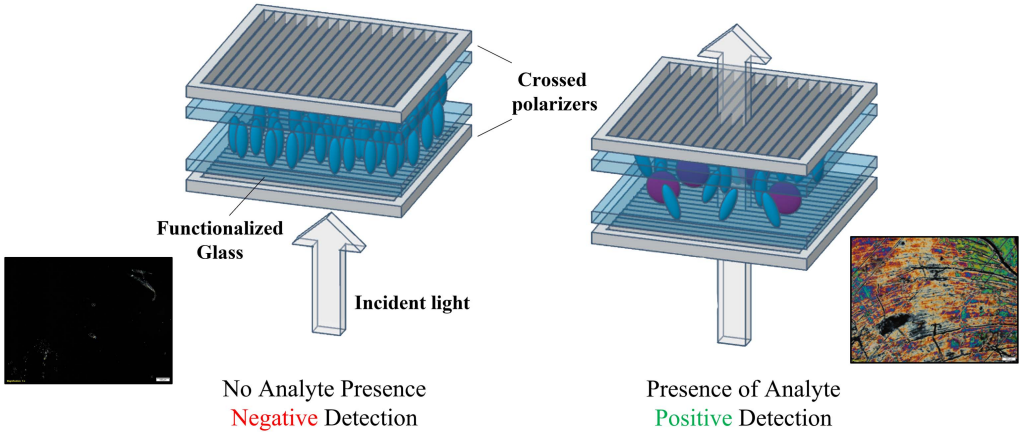

Fig. 1. Diagram representing the working principle of the LC-based sensors.

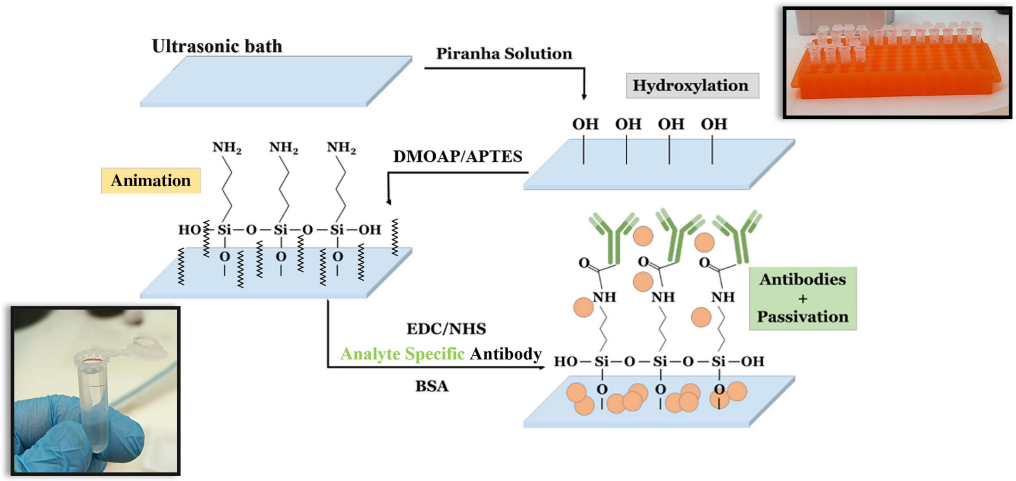

Fig. 2. The process of functionalizing the glass slides is represented in this diagram, where every step before glueing is represented [15].

functionalized cut glass slides, where they are put through several processes that contribute not only to the adherence of the specific analyte but also to the homeotropic organization of the LC molecules. First, they are put through a hydroxylation process followed by, simultaneously, an amination process and a dimethyloctadecyl[3-(trimethoxysilyl)propyl]ammonium chloride (DMOAP) treatment of said surface, promoting the adherence of the introduced molecules and helping the homeotropical alignment of the LC molecules. An analyte-specific antibody solution is used in a treatment process during the functionalization, represented in Fig. 2, and allows for the proper immobilization of the antibody and the formation of a bioreceptor layer responsible for providing specificity to the sensors. This way, only target analytes are bound to the modified glass and interact with the LC, resulting in a positive detection. This scenario is depicted in the rightmost example in Fig. 2.

For each sensor, two slides are functionalized and treated with the same solution of the same analyte, with the same concentration, and glued with a two-part epoxy glue (Instant Adhesive Ceys Araldite). The LC is finally introduced by capillary adhesion through the nonglued sides of the glass slides. The analyte detection can be performed promptly as the fabrication of the sensor is completed.

B. Setup Configuration

As mentioned, the main focus of this work was the development of a working prototype, capable of analyzing the LC-based biosensors using a digital image processing algorithm to estimate its concentrations. The general configuration of the setup was based on the working principle of the POM, which means that the analysis is done by interpreting the patterns arising from the interaction of polarized light with birefringent materials. The general configuration of the POM can be observed in Fig. 3, where the main components required for the study of birefringent materials are displayed.

The patterns created by the interaction of polarized light with the biosensors are observed by placing it between crossed dichroic polarizers, similar to the POM's configuration, and these patterns are observed through a 100× magnifying lens [22] paired with the high-quality (HQ) camera module [23], connected to a Raspberry Pi 4, as can be observed in Fig. 4. The Raspberry Pi was the preferable microcontroller, when compared with other microcontrollers (i.e., Arduino), due to its ability to handle digital image processing with a Broadcom BCM2711 SoC with a 1.8 GHz 64-bit quad-core ARM Cortex-A72 processor, as well as its native two-lane MIPI CSI camera port and its standard 40 pin GPIO header, allowing for possible lighting control. Although several combinations of lenses and cameras were tested, this HQ camera allowed for a more detailed observation of the patterns, and, given the reduced dimensions of the sensors, the magnification of the chosen lens allowed for better framing of the sensor.

As one of the main objectives was to facilitate in-the-field testing, the experimental tests were performed by fitting the

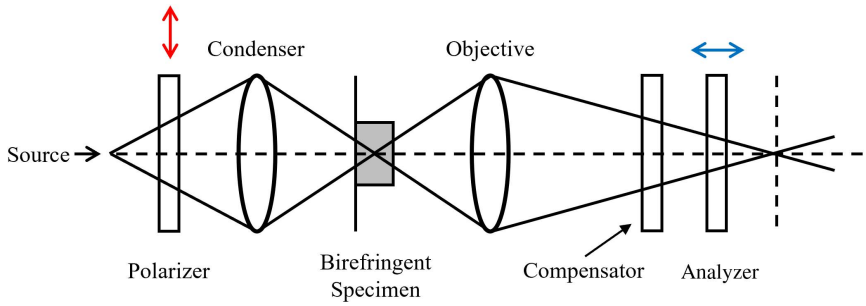

Fig. 3. Diagram of the polarized optical microscope configuration.

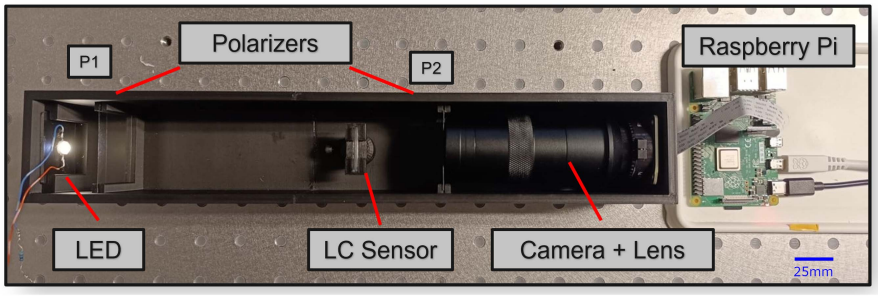

Fig. 4. Finalized prototype, with the components fitted in an encasing.

components in an optical rail, in order to optimize the distances between components, as the compactness and portability of the prototype were of the most importance. Initially, the distances between components were optimized using a reference light source, i.e., a deuterium and tungsten-halogen Sarspec light source, which also allowed for light intensity regulation and provided a stable emission for the visible light spectral range. To reduce the size of the setup, in the later stages, this light source was replaced with a light-emitting diode (LED), which also allowed for the possibility of its control via the Raspberry Pi.

So as to transport this setup more easily, recurring to a 3D-modeling software (SolidWorks), an encasing was constructed (Fig. 5), fitting all components except for the Raspberry Pi. This choice facilitates manipulating the connections to the microcontroller and reduces possible overheating issues.

Two iterations of the box were designed, as the first design showed some printing imperfections, due to the need to divide the box into separate pieces, as the 3D printer's dimensions could not fit the whole encasing. The need for a better design also came from the need to adjust the height of the sensor's support, which in the first design was not possible. The parts were printed using a 3Dfills esFil black PLA on a Bambu Lab X1-Carbon 3D printer. In Fig. 5, the final version of the encasing is shown, with a fitted hole for sunlight testing, a slot for placing the LED, and the design of the support, allowing for height adjustment and better centering of the sensor, as well as the polarizer slots. Fig. 4 shows the finalized prototype, whose dimensions when printed will be 350 mm in length, 60 mm in width, and 65 mm in height. Its final weight including the Raspberry Pi will be around 630 g.

3. RESULTS AND DISCUSSION

A. Image Processing and Component Selection

This setup utilizes the OpenCV library, which allows for the processing of the frames captured by the camera module in order to extract the relevant data from the patterns produced by light scattering on the biosensors. Various approaches were considered and tested, but the settled approach used a method of thresholding the real-time video capture. Initially, to capture the patterns with the greatest detail, the sensor was placed as close as the lens's focal distance permitted (3.0 cm from the tip of the lens), which resulted in the observation of an area of 23.62 mm^2; however, the optimal distance was defined as the sensor distance at which the frames of the video capture would align with the sides of the support (5.6 cm from the tip of the lens), as represented in Fig. 6. This would allow for better examination of the surface of the sensors.

The approach for analyte detection was based on calculating the number of colored pixels in a given region (number of colored pixels/number of total pixels), referred to as detection percentage using an adaptive thresholding method. This algorithm scans each pixel and calculates local thresholding within a defined rectangular region. It allows for better performance in noisy images and suffering from light-intensity gradients [24–26].

For the distances between the other components, it was concluded that the positioning of the light source would not compromise the detection, as the code could be altered to perform the detection at any distance. However, the farther the light source was located, the lesser the detection percentage was, although it would not interfere with the detection, as it could be mitigated with the optimization of the code. Still, as an

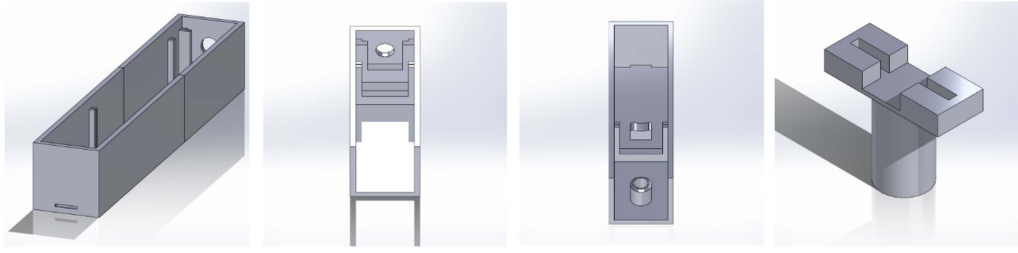

Fig. 5. 3D model of the final version encasing for the setup: (a) complete box with lid; (b) light source section, with LED slot; (c) lens section of the box; and (d) sensor support.

Fig. 6. (left) Representation of the frame alignment relative to the support. (right) Image captured by positioning the lens at an optimal distance, for an *E. coli* sensor with a concentration of 2.69×10^3 CFU/mL.

important concern of this setup was to reduce its size, the light source was placed 165 mm from the lens. Regarding the polarizers, it was found that the one placed between the sensor and the camera must be placed as close to the lens as possible, due to some distortion of the pattern when the polarizer was positioned closer to the sensor. This could be caused by beam divergence promoted by misalignment of the LC's molecular structure [27].

When preparing the biosensors, the processes are mainly focused on the center of the glass slides; further, to ensure that the detection by the algorithm is not affected by the beam divergence, the analysis area was limited to a circular region in the center of the frame. To reduce possible inaccuracies in the detection, the code was designed to require the adjustment of the detected region to the width of the sensors, resulting in a pixel detection represented in Fig. 7.

The direction in which the sensor is placed in the support could introduce some errors to the detection, and thus a study of the influence of its placement was performed. The test consisted of registering the detection percentage for the sensors' four possible placement positions. The results in Table 1 show the detection was not significantly affected by the positioning of the sensors but rather by the circular mask width adjustment.

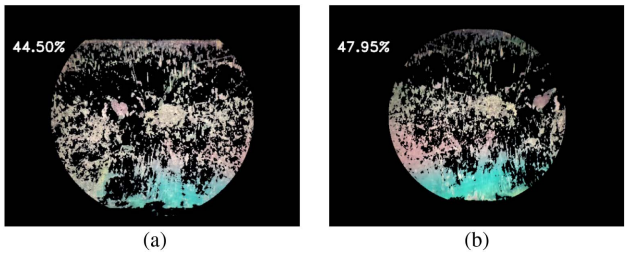

(a) (b)

Fig. 7. Region of detection for an *E. coli* biosensor with a concentration of 3.84 CFU/mL and a width of 6.4 mm: (a) without and (b) with the width adjustment.

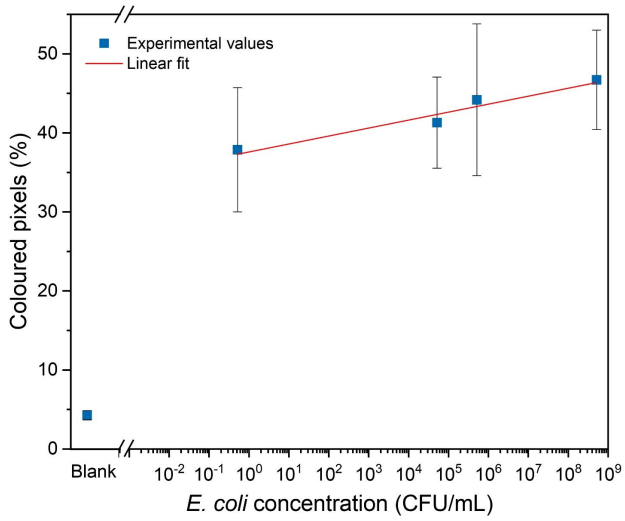

Fig. 8. Fit for the selected batch of *E. coli* biosensors, for the concentration with the percentage of colored pixels. The X axis is on a logarithmic scale.

B. Biosensor Analysis

The main objective of this work was to relate the percentage calculated by the algorithm with the real concentration values of the analyte suspensions used to fabricate each sensor. For that, a batch of the several prepared was selected, which was considered the most accurate regarding the percentage values observed, to find the curve fit, which could better estimate a concentration value. The results were obtained using the final setup (see Fig. 4).

Based on the obtained results, a logarithmic fit was expected to be the most logical curve fitting, as supported by the literature [28]. This was because larger concentrations of bacteria were observed to result in a slower rate of increase in percentages. The fits obtained were used to compare the data sets but are not depicted in the graphs because they were found to be unreliable in estimating concentrations. The graph in Fig. 8 shows the results, for which a fit was found represented by the expression $y = 1.10 \times \log_{10} x + 37.29$ with a sensitivity of $1.01\% \pm 0.17\%/\log_{10}(\text{CFU/mL})$; thus, it was integrated into the code in order to estimate the concentrations in real-time, as will be shown later.

During the development of the detection code, as well as the component selection, several sensors were fabricated. When testing some older sensors produced, there was a noticeable change in their pattern, which was observable to the naked eye. As a way of testing for how long the sensors could be accurately measured (just for statistical analysis and improving our detection code), the available *E. coli* sensors were measured using the experimental setup on two separate occasions, one month apart. The results in the following table (Table 2) were

Table 1. Percentage of Colored Pixels for Each Possible Orientation

Orientation	1	2	3	4
E. coli percentage (%)	47.55 ± 0.07	47.19 ± 0.05	46.69 ± 0.08	46.78 ± 0.44

Table 2. Change in the Measured Percentage of Colored Pixels for a Time Window of 1 Month[a]

Sensor	Concentration (CFU/mL)	Change in Detection (%)
E1	3.84	13.40 ± 11.72
E3	3.84×10^3	7.20 ± 5.77
E6	3.84×10^6	2.02 ± 0.77

[a]Note: Nine sensors in total were tested; three sensors of each concentration.

registered for three sensors of each concentration (nine sensors in total), and the change in detection is the difference in the percentage for the average of those three sensors. The sensors used in this particular analysis were tested at three distinct concentrations to observe the significant differences in such orders of magnitude. From the results in Table 2, it can be observed that, for LC-based sensors with a lower concentration of analytes, there is a greater percentage change, which could be explained by the change in the LC's general orientation, as lower concentrations promote a lower disturbance of the LC's directional alignment leading to a reorientation of the molecules. It can be concluded that the results after one month cannot be considered accurate, however; the aim of our approach is to take the measurement instantly.

C. Selectivity Test

Based on the antibody used during the functionalization process of the glass slides, the LC-based biosensors are designed and optimized to detect a single type of analyte. In order to demonstrate this selectivity, a limited set of glass slides was prepared using two additional bacteria, during the fabrication of the batch of sensors from the previous section using *E. coli* antibody: *Acinetobacter* (D6), which causes pneumonia, and *Bacillus* (O26), which is pathogenic to humans and is another bacterium linked to food-related infections.

As it can be concluded from the results in the graph in Fig. 10 and from the examples in Fig. 9, the detection of *E. coli* bacteria is more abundant when compared with the other tested strains for similar concentrations. The three bacteria arrived on the same day, with *Bacillus* O26 (3.14×10^8 CFU/mL) and *E. coli* ATTC35218 (5.16×10^8 CFU/mL) in LB growth medium and *Acinetobacter* D6 (4.22×10^8 CFU/mL) in marine growth medium. The difference in detection can be explained by the process of sensor fabrication, as the specific antibody used will only capture *E. coli* strains of O and K types. The values displayed on the graph are for the average detection of three sensors for each bacterium.

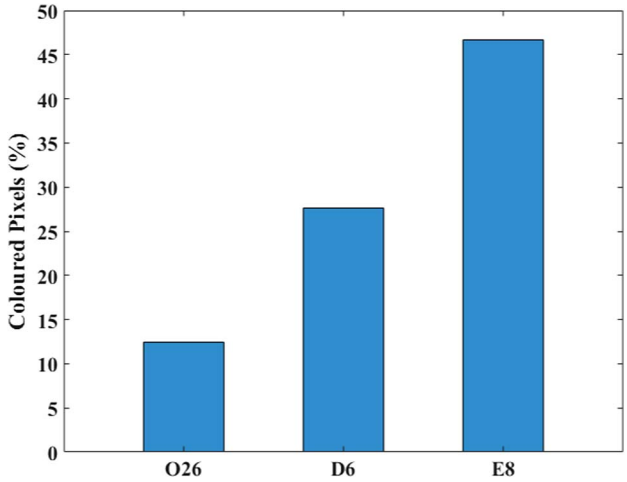

Fig. 10. Bar graph for the average percentage for *Bacillus* (O26), *Acinetobacter* (D6), and *E. coli* (E8).

D. Sunlight Testing

To demonstrate a possible improvement in the compactness and simplicity of the setup, the light source was substituted for sunlight by removing the LED, letting outside light pass through the fitted hole, as can be seen in Fig. 11. This experiment was performed by angling the box at two different times of the day, one in the morning and the other at real noon (when the Sun is at its highest point, according to SunCalc.org), with multiple inclinations in the azimuth of the Sun, which resulted in the data displayed in the graph in Fig. 12.

The peaks in both curves correspond to when the setup directly points to the Sun at that time of day. The website states that the Sun's height at 8:30 was 24.77° in the location where the measurements were made and based on the setup, the highest percentage was attained at an angle of 26.50°. Similarly, it can be observed during noon the setup's maximum percentage was 73.80°, and the peak intensity altitude was 70.47°. These results demonstrate that, through some changes in the algorithm, allowing the calculations to consider the height of the Sun, sunlight could be a viable light source.

E. Graphical User Interface

For a more user-friendly interaction with the setup, a graphical user interface (GUI) was designed, which displayed the estimated concentration on the top left corner, while also allowing to save the detection image with the printed value. It also

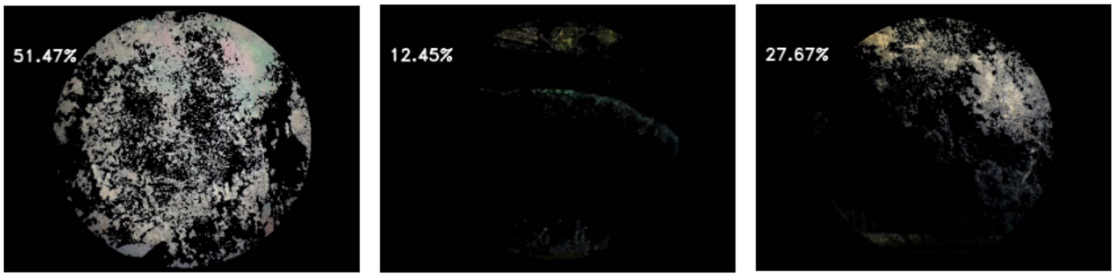

(a) (b) (c)

Fig. 9. Detection of the sensors for (a) *E. coli* ATTC35218 (E8); (b) *Bacillus* (O26); and (c) *Acinetobacter* (D6).

(a) (b)

Fig. 11. (a) Portion of the 3D-printed box design to let sunlight reach the sample. (b) Equipment used to conduct the testing outdoors.

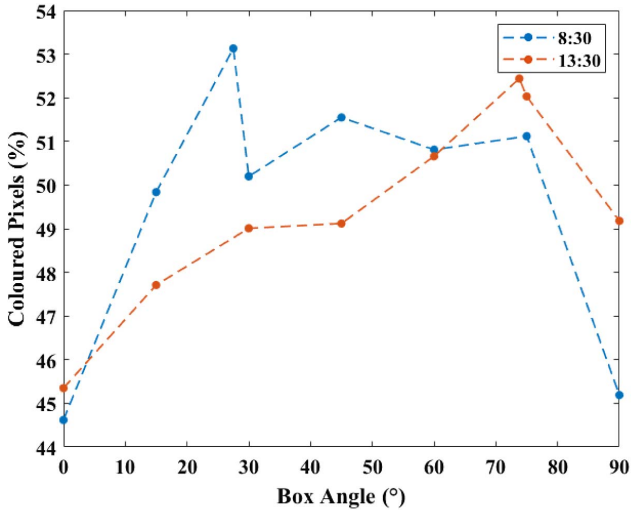

Fig. 12. Graph displaying the percentage of colored pixels detected at 8:30 and 13:30 concerning the box's angle of inclination.

permits toggling "on" and "off" of the LED if connected to the Raspberry Pi GPIO. The GUI further allows the user to input the sensor's width to fit the circular mask, which is calculated based on the pixel distance in relation to the real distance observed in the image. In Fig. 13, there are some examples of the working GUI. The GUI was made to support multiple analyte detection so that, with additional data collection in the future, a more comprehensive study of water quality could be conducted using only this setup.

4. CONCLUSIONS

A novel setup for in-the-field tests is presented in this paper. This prototype takes inspiration from the working principle of the POM while improving on its transportability, thus allowing for a faster detection mechanism when analyzing these types of LC-based biosensors, by reducing the size of its components and calculating a real-time estimation of the analyte concentration. However, the results obtained show the early stage of the prototype. The sensitivity of

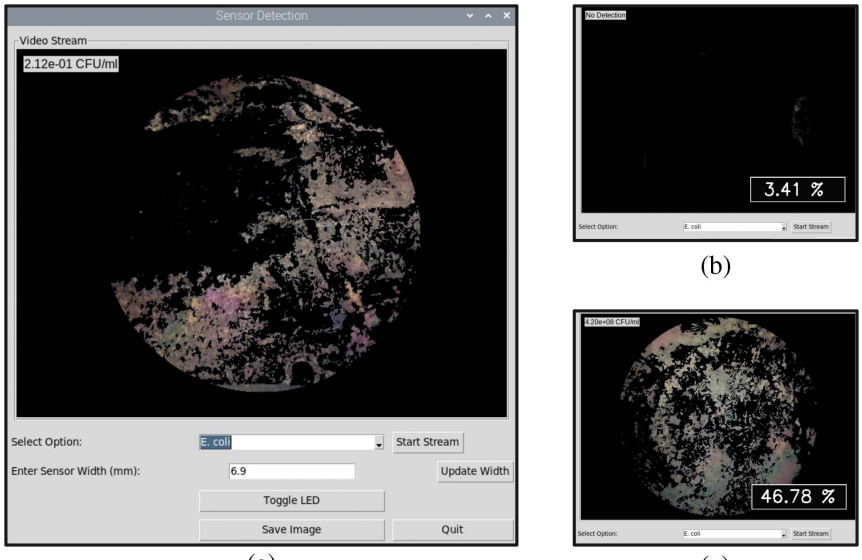

(a) (b) (c)

Fig. 13. Example of the analysis with the GUI. (a) Lower concentration *E. coli* sensor (2.12×10^{-1} CFU/mL, corresponding to 36.55%). (b) Control sensor. (c) Higher concentration *E. coli* sensor (4.20×10^{8} CFU/mL).

1.01% ± 0.17%/$\log_{10}$ (CFU/mL) for the *E. coli* sensors could be improved by standardizing the fabrication of said sensors, therefore improving the accuracy of the estimation, as in its current state the main focus was to estimate the order of magnitude of the concentrations. Although many tests were performed for the optimization of the distances, the components could differ in their positions, as long as the algorithm is constructed regarding those changes. The settled positions allowed for a reduced size of the setup, which was the most relevant concern.

The novelty on this prototype comes from the approach on simplifying the analysis process in aquaculture systems, providing a new and faster method of estimating *E. coli* concentration in bivalve production, building upon the use of LC-based immunosensors, which already provide a fast, less invasive, highly specific, and sensitive form of detection. The reduced dimensions of this sensor (35 cm × 6 cm × 6.5 cm) result in its increased portability, allowing for a faster *in situ* response, which is further improved by the possibility of using sunlight as a light source and also making room for a more simplified approach toward its design. The faster the detection of pathogenic bacteria, the lesser the possibility of its spread; therefore, the contribution will provide a timely threat response.

In future research, in order to obtain better sensitivity results, the most obvious path is to implement machine learning components in the analysis of the detection results, which will most definitely lead to better sensitivity results. In addition, another future research will explore the changes in the sensor patterns after a few days to understand the potential reasons of such a considerable change in the percentage for a lower concentration of analytes as reported here after one month. However, this paper outlines the initial research for faster, instant measurement, and more portable water analysis alternatives.

Funding. European Commission (CZ.10.03.01/00/22-003/0000048); Fundação para a Ciência e a Tecnologia (PTDC/EEI-EEE/0415/2021, CICECO (UIDB/50011/2020, UIDP/50011/2020, LA/P/0006/2020); VSB-Technical University of Ostrava (SP2025/039); FCT/MCTES (UI/BD/153066/2022).

Acknowledgment. This work was developed within the scope of the projects CICECO (LA/P/0006/2020, UIDB/50011/2020, and UIDP/50011/2020) financed by national funds through the Portuguese Science and Technology Foundation/MCTES (FCT I.P.). The research was also co-funded by the financial support of the European Union under the REFRESH – Research Excellence For REgion Sustainability and High-tech Industries (project No. CZ.10.03.01/00/22-003/0000048) via the Operational Programme Just Transition. This work was also supported by the Ministry of Education, Youth, and Sports of the Czech Republic conducted by the VSB-Technical University of Ostrava, under grant No. SP2025/039. M. S. Soares acknowledges FCT/MCTES for the PhD fellowship grant UI/BD/153066/2022. N. Santos acknowledges FCT I.P. for the research action 2022.04595.CEECIND (GraFiberSens project).

Disclosures. The authors declare no conflicts of interest.

Data Availability. Data underlying the results presented in this paper are not publicly available at this time but may be obtained from the authors upon reasonable request.

REFERENCES

1. R. Gupta, *Foodborne Infectious Diseases* (Elsevier, 2017), pp. 13–28.
2. World Health Organization (WHO), "Estimating the burden of foodborne diseases," https://www.who.int/activities/estimating-the-burden-of-foodborne-diseases. Accessed 08-04-2024.
3. World Health Organization (WHO), "*E. coli*," https://www.who.int/news-room/fact-sheets/detail/e-coli. Accessed 09-04-2024.
4. European Food Safety Authority (EFSA), "World Food Safety Day 2024 — commission.europa.eu," https://commission.europa.eu/news/world-food-safety-day-2024-2024-06-07_en. Accessed 14-09-2024.
5. FAO, *The State of World Fisheries and Aquaculture* (FAO, 2022).
6. "IPMA - zonas de produção moluscos bivalves," https://www.ipma.pt/pt/bivalves/zonas/. Accessed 18-09-2024.
7. J. Oliveira, F. Castilho, Â. Cunha, *et al.*, "Bivalve harvesting and production in Portugal: an overview," J. Shellfish Res. **32**, 911–924 (2013).
8. A. C. Braga, S. M. Rodrigues, H. M. Lourenço, *et al.*, "Bivalve shellfish safety in Portugal: variability of faecal levels, metal contaminants and marine biotoxins during the last decade (2011–2020)," Toxins **15**, 91 (2023).
9. M. B. Sultan, A. H. Anik, and M. M. Rahman, "Emerging contaminants and their potential impacts on estuarine ecosystems: are we aware of it?" Mar. Pollut. Bull. **199**, 115982 (2024).
10. A. M. Larsen, F. Scott Rikard, W. C. Walton, *et al.*, "Effective reduction of *Vibrio vulnificus* in the Eastern oyster (*Crassostrea virginica*) using high salinity depuration," Food Microbiol. **34**, 118–122 (2013).
11. "IPMA - Bivalves - ponto de situação," https://www.ipma.pt/pt/bivalves/index.jsp. Accessed 10-09-2024.
12. M. Luna, I. Llorente, and L. Luna, "A conceptual framework for risk management in aquaculture," Mar. Policy **147**, 105377 (2023).
13. M. J. Stephen and J. P. Straley, "Physics of liquid crystals," Rev. Mod. Phys. **46**, 617–704 (1974).
14. P. de Gennes and J. Prost, *The Physics of Liquid Crystals*, International Series of Monographs on Physics (Clarendon, 1993).
15. M. S. Soares, R. G. Sobral, N. Santos, *et al.*, "Liquid crystal-based immunosensor for the optical detection of escherichia coli at low concentration levels," IEEE Sens. J. **24**, 8848–8856 (2023).
16. X. Zhan, Y. Liu, K. L. Yang, *et al.*, "State-of-the-art development in liquid crystal biochemical sensors," Biosensors **12**, 577 (2022).
17. A. Bezrukov and Y. Galyametdinov, "Orientation behavior of nematic liquid crystals at flow-wall interfaces in microfluidic channels," Coatings **13**, 169 (2023).
18. A. Locke, S. Fitzgerald, and A. Mahadevan-Jansen, "Advances in optical detection of human-associated pathogenic bacteria," Molecules **25**, 5256 (2020).
19. P. Wang, H. Sun, W. Yang, *et al.*, "Optical methods for label-free detection of bacteria," Biosensors **12**, 1171 (2022).
20. "Polarizing microscopes," https://microscopecentral.com/collections/polarizing. Accessed 30-09-2024.
21. Spach Optics, "Used & reconditioned microscopes for sale," https://www.spachoptics.com/default.asp. Accessed 30-09-2024.
22. waveshare.com, "100X industrial microscope lens, C/CS-mount, compatible with Raspberry Pi HQ camera | 100X microscope lens for Pi," https://www.waveshare.com/100x-microscope-lens-for-pi.htm. Accessed 03-06-2024.
23. Raspberry Pi, "Raspberry Pi documentation - cameras," https://www.raspberrypi.com/documentation/accessories/camera.html. Accessed 14-05-2024.

24. R. Gonzalez and R. Woods, *Digital Image Processing* (Pearson, 2018).
25. R. Klette, *Concise Computer Vision: An Introduction into Theory and Algorithms* (Springer, 2014).
26. OpenCV - Open Source Computer Vision, "OpenCV: Image Thresholding — docs.opencv.org," https://docs.opencv.org/4.x/d7/d4d/tutorial_py_thresholding.html. Accessed 04-04-2024.
27. A. Habibpourmoghadam, L. Jiao, V. Reshetnyak, *et al.*, "Optical manipulation and defect creation in a liquid crystal on a photoresponsive surface," Phys. Rev. E **96**, 022701 (2017).
28. T.-K. Chang, M.-J. Lee, and W. Lee, "Quantitative biosensing based on a liquid crystal marginally aligned by the PVA/DMOAP composite for optical signal amplification," Biosensors **12**, 218 (2022).